Journal of Inflammation Research

Dovepress
open access to scientific and medical research

Open Access Full Text Article

ORIGINAL RESEARCH

HMGB1-Induced Hepatocyte Pyroptosis Expanding Inflammatory Responses Contributes to the Pathogenesis of Acute-on-Chronic Liver Failure (ACLF)

Weixin Hou[1–4]
Xiaoyi Wei[1,2]
Jiajun Liang[1–4]
Peng Fang[5]
Chongyang Ma[1,2]
Qiuyun Zhang[1,2,*]
Yanbin Gao[3,4,*]

[1]Department of Hepatology, School of Traditional Chinese Medicine, Capital Medical University, Beijing, People's Republic of China; [2]Department of Hepatology, Beijing Key Laboratory of Traditional Chinese Medicine Collateral Disease Theory Research, Capital Medical University, Beijing, People's Republic of China; [3]Department of Endocrinology, School of Traditional Chinese Medicine, Capital Medical University, Beijing, People's Republic of China; [4]Department of Endocrinology, Beijing Key Laboratory of Traditional Chinese Medicine Collateral Disease Theory Research, Capital Medical University, Beijing, People's Republic of China; [5]Department of Infectious Diseases, First Affiliated Hospital of Zhejiang Chinese Medical University, Hangzhou, Zhejiang Province, People's Republic of China

*These authors contributed equally to this work

Correspondence: Qiuyun Zhang; Yanbin Gao
School of Traditional Chinese Medicine, Capital Medical University, No. 10 You An Men Wai, Xi Tou Tiao, Feng Tai District, Beijing, 100069, People's Republic of China
Tel +86 10 8391 1638; +86 10 8391 1720
Email 19970059@ccmu.edu.cn; gyb@ccmu.edu.cn

Background: Acute-on-chronic liver failure (ACLF) is a critical disease with a high fatality rate. Immune dysfunction and inflammatory responses are key risk factors in ACLF. Pyroptosis is a form of programmed cell death characterized by the release of inflammatory cytokines, which causes the strong inflammatory responses. High mobility group box-1 (HMGB1) could induce pyroptosis and is closely related to ACLF. However, the role of HMGB1-induced hepatocyte pyroptosis in ACLF has never been proposed; whether HMGB1-induced hepatocyte pyroptosis participates in the development of ACLF and the mechanisms involved are barely understood.

Purpose: This study aimed to clarify the roles of HMGB1-induced hepatocyte pyroptosis in ACLF and the molecular mechanisms involved.

Methods: Wistar rats were randomly divided into five groups, viz.: Normal, ACLF model, HMGB1 inhibitor, Caspase-1 inhibitor, and HMGB1 inhibitor+Caspase-1 inhibitor groups. The ACLF rat model was established using 40% carbon tetrachloride-induced liver fibrosis, followed by D-galactosamine and lipopolysaccharide joint acute attacks. The liver function, coagulation function and pathological damage of rats in each group were evaluated. The biological mechanisms of HMGB1-induced pyroptosis and the release of inflammatory cytokines were investigated using Western blot, quantitative real-time PCR (RT-qPCR), immunofluorescence, enzyme-linked immunosorbent assay (ELISA), and terminal deoxynucleotidyl transferase dUTP nick end labeling (TUNEL) assay.

Results: The liver function and coagulation function of ACLF rats were seriously impaired; liver tissue showed massive or submassive necrosis, accompanied by inflammatory cell infiltration; the percentage of pyroptotic hepatocytes significantly increased, and a large number of inflammatory cytokines were released. The expression levels of pyroptosis-related genes and proteins in liver tissues and serum significantly increased. But these phenomenons were improved by the inhibition of HMGB1, and the dual inhibition of HMGB1 and Caspase-1 showed a stronger effect.

Conclusion: The findings indicate, for the first time, that pyroptosis is a crucial pathophysiological event of ACLF involved in its pathogenesis, and HMGB1-induced hepatocyte pyroptosis expands inflammatory responses to aggravate ACLF, suggesting that it may be a potential therapeutic target for ACLF treatment.

Keywords: HMGB1, pyroptosis, inflammatory response, molecular mechanism of ACLF, ACLF treatment

Received: 2 September 2021
Accepted: 10 December 2021
Published: 23 December 2021

Introduction

Acute-on-chronic liver failure (ACLF) is a severe life-threatening disease that develops extremely rapidly, with a short-term mortality rate as high as 50%-90%.[1] There is no consensus definition of ACLF yet between Eastern and Western medicine. The "Guideline for Diagnosis and Treatment of Liver Failure (2018 Edition)" states that ACLF refers to liver failure manifestations, such as acute jaundice and coagulation dysfunction, caused by various inducements on the basis of chronic liver disease, which can combine with multiple complications such as hepatic encephalopathy, ascites, infection, etc.[2,3] The development of ACLF is a multi-factor, multi-link, and multi-pathway evolutionary process, the mechanism is extremely complex and has not been fully elucidated, but it is generally believed that immune dysfunction and inflammatory response are key factors in ACLF.[4,5]

High mobility group box1 (HMGB1) is an evolutionarily conserved nuclear DNA-binding protein that exists widely in eukaryotic cells. When exogenous microorganisms invade or endogenous tissue damage occurs, HMGB1 is released to the outside of the cell as a stress signal and inflammatory mediator. Once translocated to the outside of the cell, HMGB1 takes on a new identity as a damage-associated molecular pattern (DAMP) molecule, and activates immune cells to produce tumor necrosis factor-α (TNF-α), interleukin-1 β (IL-1β), and other pro-inflammatory factors, which trigger inflammatory responses,[6,7] and plays a key role in the development of ACLF.[8,9] HMGB1 plays a crucial role in the common pathway of infectious and aseptic inflammatory responses, and initiates pyroptosis by binding with the receptor for advanced glycation end-products (RAGE) or Toll-like receptor 4 (TLR4).[10–12]

Pyroptosis is a Caspase-1- and/or Caspase-4/-5/-11-dependent pattern of inflammation-related programmed death, which is mediated by inflammasomes and Gasdermin D (GSDMD).[13,14] When endogenous and exogenous stimuli activate Caspase-1 and/or Caspase-4/-5/-11 through different signaling pathways, GSDMD is cleaved to form a peptide containing the N-terminal domain (GSDMD-N), resulting in cells swelling and rupture to form a multitude of pores of diameter between 1.1–2.4 nm in the membrane.[15] Intracellular substances such as lactate dehydrogenase (LDH) and electrolytes flow out through the cell membrane, and pro-IL-1β and pro-IL-18 lyse to induce the synthesis and release of a large number of inflammatory factors and adhesion molecules, expand local and systemic inflammatory responses, and further aggravate tissue damage.[16]

As a DAMP molecule, HMGB1 can induce pyroptosis and plays an important role in ACLF. Pyroptosis is a kind of programmed cell death characterized by the release of inflammatory cytokines, which triggers a strong inflammatory response. Pyroptosis plays an important role in the process of cell and tissue damage and necrosis. The fundamental pathological mechanism of ACLF is immune dysfunction and inflammatory response, which is very similar to the characteristics of pyroptosis. However, whether and how HMGB1-induced hepatocyte pyroptosis is involved in the development of ACLF are worth studying in depth.

In this study, we established an ACLF rat model and administered the HMGB1 inhibitor, Caspase-1 inhibitor, and combined intervention of the HMGB1 inhibitor and Caspase-1 inhibitor to investigate the biological mechanism of HMGB1-induced hepatocyte pyroptosis and inflammatory responses in ACLF rats, and evaluate the effect of HMGB1-induced hepatocyte pyroptosis and inflammatory responses on ACLF. This study demonstrates, for the first time, the role of pyroptosis in ACLF, and elucidates the new pathogenesis of ACLF, which will provide a reliable theoretical basis for HMGB1-induced pyroptosis as an effective target for the treatment of ACLF.

Materials and Methods

Animal Materials

Male Wistar rats (weighing 180–200 g, n=51) were purchased from Beijing Vital River Laboratory Animal Technology Co., Ltd., Beijing, China. Three rats each were kept in an individually ventilated cage (IVC) at the Laboratory Animal Center of Capital Medical University, Beijing, China under specific-pathogen-free (SPF) conditions. The rats were free to eat and drink at room temperature of 22–25 °C and humidity of (50.0±2.0)%. The lights were turned on every 12 h for illumination.

Animal Experiments

Establishment of ACLF Model

After one week of adaptive feeding, the rats were randomly divided into the normal group (n=9) and treatment groups (n=42), according to the random number table method. The treatment groups included the ACLF model group (n=12), the HMGB1 inhibitor group (n=10), the Caspase-1 inhibitor group (n=10), and the HMGB1

inhibitor+Caspase-1 inhibitor group (n=10). The ACLF rat model was established in the treatment groups according to a previously reported method,[1,17] and with the following operations performed:

Step 1: Establishment of the liver fibrosis model: The rats in treatment groups were intraperitoneally injected with 40% carbon tetrachloride (CCl4) and vegetable oil mixture (1.5 mL/kg) twice a week for 10 weeks. Subsequently, liver tissue biopsy was performed, and the results of masson's trichrome (MT) and hematoxylin and eosin (HE) staining confirmed the occurrence of liver fibrosis (Figure S1). Step 2: Establishment of the ACLF model: On this basis, the treatment groups were simultaneously intraperitoneally challenged with D-galactosamine (500 mg/kg) and lipopolysaccharide (100 μg/kg) (D-GalN/LPS) for acute attacks to establish the ACLF model. Twenty-nine rats survived these operations (including ACLF model group (n=8), HMGB1 inhibitor group (n=7), Caspase-1 inhibitor group (n=7) and HMGB1 inhibitor+Caspase-1 inhibitor group (n=7)). The normal group was intraperitoneally injected with the same dosage of 0.9% physiological saline as in the treatment groups.

Rats in each group were sacrificed 12 h after the acute attacks, liver tissue and blood samples were collected for subsequent experiments.

Intervention Treatment

One week before the acute attacks, the HMGB1 inhibitor group was intraperitoneally injected with glycyrrhizin (GLY, 50 mg/kg),[18,19] the Caspase-1 inhibitor group was intragastrically injected with VX-765 (50 mg/kg),[20–22] and the HMGB1 inhibitor+Caspase-1 inhibitor group was intraperitoneally injected with GLY (50mg/kg),[18,19] followed by administration of VX-765 (50 mg/kg) via oral gavage,[20–22] the normal group and the ACLF model group were intraperitoneally injected with the same volume of 0.9% physiological saline as the HMGB1 inhibitor group. The above operations were performed once per day for 1 week.

Assessment of Liver Function

After the collection of the blood of rats in each group, the samples were undisturbed and kept at room temperature for 4 h, then centrifuged at 4000 rpm for 15 min at 4 °C to separate the serum. The levels of serum alanine aminotransferase (ALT), aspartate aminotransferase (AST), total bilirubin (TBIL) and albumin (ALB) of each sample were detected using a Hitachi 7600 automatic biochemical analyzer (Hitachi, Tokyo, Japan).

Coagulation Function Test

The blood samples were anticoagulated with sodium citrate, and centrifuged at 4000 rpm for 15 min at 4 °C to collect the plasma. The levels of prothrombin time (PT) and international normalized ratio (INR) in plasma of rats in each group were measured with the Beckman Coulter ACL-TOP 700 Coagulation Analyzer (Beckman Coulter, Inc., Chaska, MN, USA) within 2 h.

LDH Release Assay

The serum of each group was collected and the LDH Release Assay Kit (Leadman Group Co., Ltd., Beijing, China) was used to determine the serum LDH level according to the manufacturer's instructions.

Histological Examinations

The liver tissues were fixed in 4% paraformaldehyde, embedded in paraffin, and cut into 4 μm thick slices, which were stained with HE and MT, and scanned with the Pannoramic SCAN II slide scanner (3DHISTECH Ltd., Budapest, Hungary). CaseViewer software was used to observe the pathological damage of liver in each group, and obtain images.

Transmission Electron Microscopy (TEM)

The tissues were fixed with 2.5% glutaraldehyde for 2 h and osmium acid for 1 h, and embedded in epoxy resin. Ultra-thin sections (70 nm in thickness) were cut and stained with saturated uranyl acetate and lead citrate, and the ultra-structure of hepatocytes were observed and photographed by Hitachi HT7700 TEM (Hitachi, Tokyo, Japan).

Immunofluorescent Staining

For immunofluorescent staining, paraffin sections (4 μm) of liver tissue were deparaffinized with xylene and ethanol, antigen retrieval was performed with citrate buffer solution. The tissue sections were sealed with 10% normal goat serum for 1 h, then incubated overnight at 4 °C with anti-HMGB1antibody (1:250, ab79823, Abcam, Cambridge, UK) or anti-GSDMD antibody (1:200, ab219800, Abcam, Cambridge, UK). After washing with PBS, the sections were incubated with Rhodamine (TRITC)-conjugated Goat Anti-Rabbit IgG (H+L) (1:50, SA00007-2, Proteintech, Chicago, IL, USA) or Fluorescein (FITC)-conjugated

Affinipure Goat Anti-Rabbit IgG (H+L) (1:50, SA00003-2, Proteintech, Chicago, IL, USA) at 37 °C for 2 h. After washing with PBS, the sections were covered with an anti-fade mounting medium with 4′,6-diamidino-2-phenylindole (DAPI) and examined with Leica TCS SP8 STED 3X Super-Resolution Confocal Microscope (Leica microsystems, Wetzlar, Germany).

For further observation of hepatocyte pyroptosis in liver tissue, triple-immunostaining of active Caspase-1, terminal deoxynucleotidyl transferase dUTP nick end labeling (TUNEL) and ALB (hepatocyte marker) were performed. Active Caspase-1+/TUNEL+/ALB+ triple-positive cells were termed as pyroptotic hepatocytes, and the percentage of triple-positive cells was calculated. Ten fields were randomly examined in each liver section and the mean values were taken for statistical analysis.

Western Blotting Analysis

The liver tissues were lysed with RIPA buffer containing protease and phosphatase inhibitors, homogenized and centrifuged to collect the total proteins. Nuclear and cytoplasmic proteins extraction kits (Beyotime Biotechnology, Shanghai, China) were used to isolate nuclear and cytoplasmic proteins according to the manufacturer's instructions. Then the sample concentration was uniformly adjusted to 3 μg/μL. Proteins were separated by SDS polyacrylamide gel electrophoresis (SDS-PAGE) and transferred to polyvinylidene difluoride (PVDF) membrane, sealed with 5% skimmed milk powder for 1 h, and then incubated with a diluted solution of anti-HMGB1 (1:20,000, ab79823, Abcam, Cambridge, UK), anti-TLR4 (1:400, sc-293072, Santa Cruz Biotechnology, Santa Cruz, CA, USA), anti-RAGE (1:500, sc-365154, Santa Cruz Biotechnology, Santa Cruz, CA, USA), anti-NF-κB (1:1000, #8242, Cell Signaling Technology, Danvers, MA, USA), anti-apoptosis-associated speck-like protein containing a caspase recruitment domain (anti-ASC) (1:400, sc-514414, Santa Cruz Biotechnology, Santa Cruz, CA, USA), anti-IL-18 (1:2000, ab191860, Abcam, Cambridge, UK), anti-IL-1β (1:400, sc-12742, Santa Cruz Biotechnology, Santa Cruz, CA, USA), anti-NLRP3 (1:1000, ab263899, Abcam, Cambridge, UK), anti-GSDMD (1:1000, ab219800, Abcam, Cambridge, UK), anti-GSDMD-N (1:800, SAB2108448, Sigma-Aldrich, St. Louis, MO, USA), anti-Caspase-1 (1:1000, ab179515, Abcam, Cambridge, UK), anti-Histone H3 (1:2000, #4499, Cell Signaling Technology, Danvers, MA, USA), or anti-GAPDH (1: 5000, G0100, LabLead Bio-Technology Co., Ltd., Beijing, China) at 4 °C overnight. After washing with 1xTBST 4 times, the membranes were incubated with Goat anti-Mouse IgG (H+L)-HRP (1:5000, S0100, LabLead Bio-Technology Co., Ltd., Beijing, China), Goat anti-Rabbit IgG (H+L)-HRP (1:5000, S0101, LabLead Bio-Technology Co., Ltd., Beijing, China), or mouse anti-Armenian hamster IgG-HRP (1:5000, sc-2789, Santa Cruz Biotechnology, Santa Cruz, CA, USA) at room temperature for 1 h; the target proteins were observed using the Vilber FUSION FX6 XT gel chemiluminescence imaging analysis system (Vilber Lourmat, Marne La Vallee, France). Densitometric analysis of the Western blots was performed with ImageJ software[23] and compared with the internal control (anti-Histone H3 or anti-GAPDH antibody) to determine the difference in protein expression. All experiments were repeated three times.

Enzyme-Linked Immunoassay (ELISA)

ELISA kits (Zhong Shang Bo Ao Biological Technology Co., Ltd, Beijing, China, and Kang Jia Hong Yuan Biological Technology Co., Ltd, Beijing, China) were used to determine the expression levels of HMGB1, TLR4, and RAGE in serum and of the pro-inflammatory cytokines IL-1β, IL-18, TNF-α and interleukin-6 (IL-6) in liver tissues.

Quantitative Real-Time PCR (RT-qPCR) Analysis

The total RNAs were extracted from liver tissue samples with the RNAprep pure Tissue Kit (TIANGEN biotech Co., Ltd., Beijing, China), according to the manufacturer's instructions, and the concentration of total RNAs were measured by the Pultton P200 micro volume spectrophotometer (Pultton, San Jose, CA, USA). The total RNAs were reverse-transcribed into cDNA using the FastKing RT Kit (With gDNase) (TIANGEN biotech Co., Ltd., Beijing, China). The RT-qPCR reaction system was established with the SuperReal PreMix Plus (SYBR Green) Kit (TIANGEN biotech Co., Ltd., Beijing, China), according to the manufacturer's instructions. *β-actin* was used as internal reference. The reaction conditions were 95 °C for 15 min, 40 cycles of 95 °C for 10 s, 60 °C for 20 s and 72 °C for 30 s. The gene expression was analyzed by $2^{-\Delta\Delta CT}$. All experiments were repeated three times. Primer sequences are shown in Table 1.

Table 1 Primer Sequences for RT-qPCR Analysis

Gene Name		Primer Sequences (5′ to 3′)
HMGB1	Forward	5′- CGAATGTGTCTTTAGCTAGCCCTGT-3′
	Reverse	5′- CAGACTGTACCAGGCAAGGTTAGTG-3′
Caspase-1	Forward	5′- ACTCGTACACGTCTTGCCCTCA-3′
	Reverse	5′- CTGGGCAGGCAGCAAATTC-3′
NLRP3	Forward	5′- CTGAAGCATCTGCTCTGCAACC-3′
	Reverse	5′- AACCAATGCGAGATCCTGACAAC-3′
IL-1β	Forward	5′- CCCTGAACTCAACTGTGAAATAGCA-3′
	Reverse	5′- CCCAAGTCAAGGGCTTGGAA-3′
IL-18	Forward	5′- ACTGGCTGTGACCCTATCTGTGA-3′
	Reverse	5′- TTGTGTCCTGGCACACGTTTC-3′
β-actin	Forward	5′- CCTAAGGCCAACCGTGAAA-3′
	Reverse	5′- CAGAGGCATACAGGGACAACAC-3′

Abbreviations: RT-qPCR, quantitative real-time PCR; HMGB1, high mobility group box-1; IL-1β, interleukin-1 β; IL-18, interleukin-18.

Statistical Analyses

GraphPad Prism 9 (GraphPad Software, Inc., La Jolla, CA, USA) was used for statistical analysis of experimental data. Firstly, the Shapiro–Wilk test and QQ plot (Figure S2) were used to evaluate whether the data followed normal distribution. Secondly, for data that followed normal distribution and homogeneity of variance, statistical comparison between any two groups was carried out using Student's *t*-test, whereas comparison among multiple groups was performed via one-way ANOVA, followed by the Tukey's test. For the data that were not normally distributed or had inhomogeneity of variance, statistical comparison between any two groups was done with the Mann–Whitney test, whereas comparison among multiple groups was performed with the Kruskal–Wallis test, followed by Dunn's test. *P* values denoted the statistical differences, where $P < 0.05$ showed statistical significance, and $P < 0.01$, $P < 0.001$, and $P < 0.0001$ indicating notable statistical significance.

Results

HMGB1 Was Activated in the Livers of ACLF Rats

To evaluate whether HMGB1 was activated and participated in the progression of ACLF, we determined the expression of HMGB1 in the livers of ACLF rats by Western blot, RT-qPCR, and immunofluorescence, and determined the serum HMGB1 level by ELISA. The results showed that compared with the normal group, the expression of HMGB1 in the liver cytoplasm of the ACLF model group significantly increased ($P<0.0001$), and the expression in the nucleus significantly reduced ($P=0.0068$), with HMGB1 showing obvious translocation from the nucleus to the cytoplasm (Figure 1A–C). The results of immunofluorescence further confirmed this phenomenon (Figure 1D). The transcript levels of *HMGB1* in the livers of ACLF rats were significantly higher than those of the normal group ($P=0.0002$) (Figure 1E). Compared with the normal group, the serum HMGB1 level in the ACLF model group significantly increased ($P<0.0001$), which was verified by ELISA (Figure 1F). In addition, we studied the expressions of the two receptors of HMGB1-TLR4 and RAGE-in the liver tissue and serum of ACLF rats by Western blot and ELISA, and the results showed that the expressions in the ACLF model group were significantly higher than that in the normal group (each receptor $P<0.0001$) (Figure 1G–K). To further prove that the development of ACLF was closely related to the upregulation and translocation of HMGB1, we added the HMGB1 inhibitor and the Caspase-1 inhibitor. The inhibition of HMGB1 significantly reduced the transcription level of *HMGB1* ($P=0.0008$) (Figure 1E), and the expression of HMGB1 in the cytoplasm ($P=0.0002$) (Figure 1A and C), and the phenomenon of translocation from the nucleus to the cytoplasm (Figure 1D). The expressions of TLR4 and RAGE were inhibited prominently (each $P<0.0001$) (Figure 1I–K), and the levels of HMGB1, TLR4 and RAGE in serum significantly decreased ($P<0.0001$, $P=0.0003$, $P<0.0001$) (Figure 1F–H). Inhibition of Caspase-1 decreased the levels of RAGE (ELISA: P=0.0022, Figure 1H; Western blot: $P<0.0001$, Figure 1I and K) and HMGB1 (ELISA: $P<0.0001$,

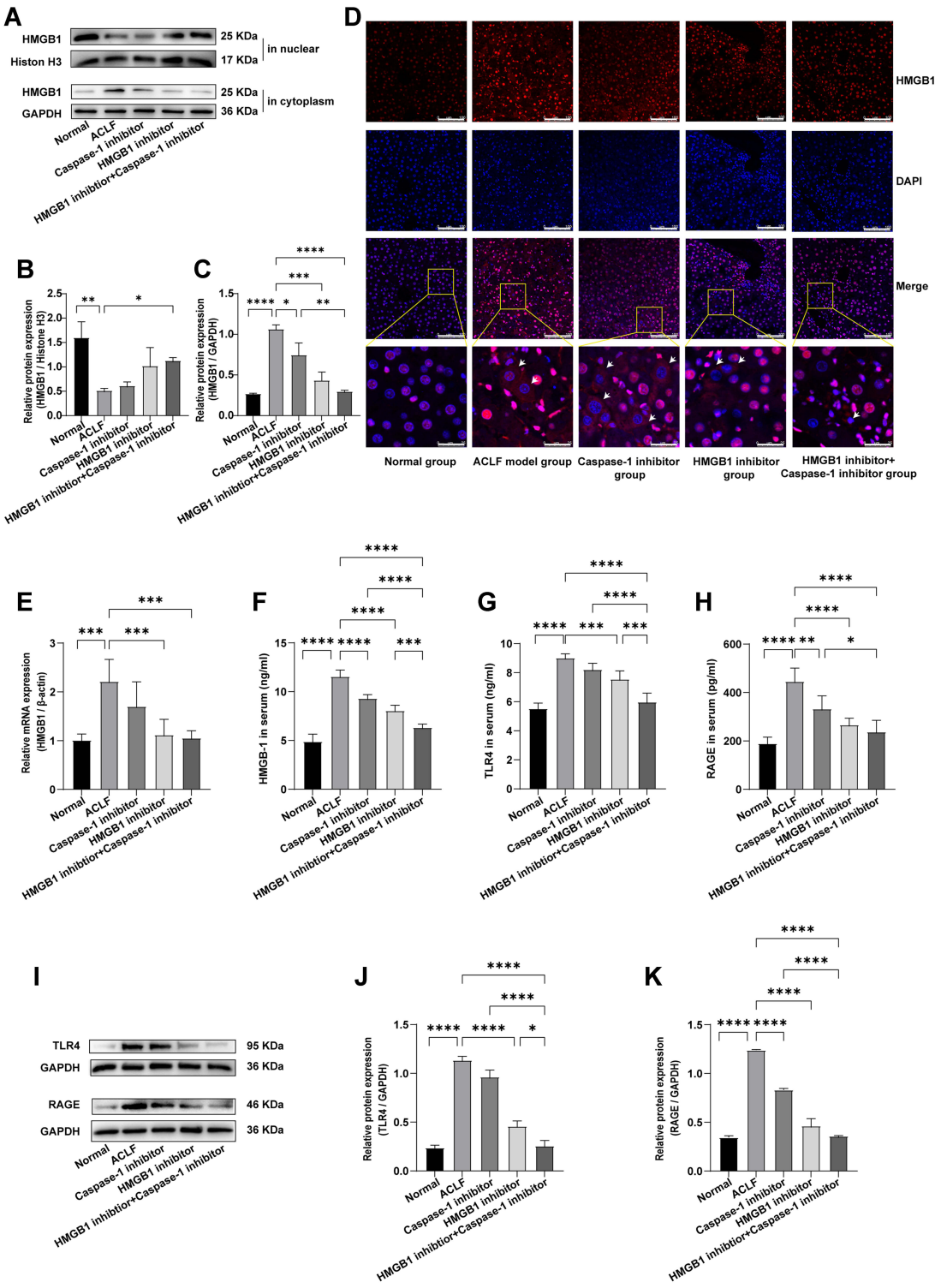

Figure 1 HMGB1 was activated in the livers of ACLF rats.

Notes: (**A**–**C**) The expression levels of HMGB1 in the nucleus and cytoplasm were detected by Western blot. Histone H3 or GAPDH were used as the loading control. n=3 per group. (**D**) The expression and translocation of HMGB1 in the liver tissues of each group were determined by immunofluorescence (magnification, ×400; scale bar=100 μm). A region is boxed randomly in each group and the boxed regions are further enlarged below (magnification, ×1600; scale bar=25 μm). The arrows indicate cells that exhibited HMGB1 translocation from the nucleus to the cytoplasm. (**E**) Relative transcripts level of *HMGB1* of rats in each group was detected by RT-qPCR. *β-actin* was used as internal reference. n=6 per group. (**F**–**H**) The levels of HMGB1, TLR4 and RAGE in serum were detected by ELISA. The normal group (n=9), the ACLF model group (n=8), the inhibitor groups (each n=7). (**I**–**K**) Western blot was used to detect the expressions of TLR4 and RAGE, and GAPDH was used as the loading control. n=3 per group. Asterisks indicate statistical significance: *P**< 0.05, *P***< 0.01, *P****< 0.001, and *P*****< 0.0001.

Abbreviations: HMGB1, High mobility group box-1; ACLF, acute-on-chronic liver failure; RT-qPCR, quantitative real-time PCR; TLR4, Toll-like receptor 4; RAGE, receptor for advanced glycation end-products; ELISA, enzyme-linked immunosorbent assay.

Figure 1F; Western blot: P=0.0183, Figure 1A and C). These results strongly suggested that HMGB1 was activated in the liver tissue of ACLF rats and participated in the progression of ACLF.

The Livers of ACLF Rats Showed Severe Hepatocyte Pyroptosis

Considering that the activation of HMGB1 is closely associated with pyroptosis, we further investigated whether pyroptosis occurred in liver tissues of ACLF rats. GSDMD-N is the executive protein of pyroptosis. When pyroptosis occurs, GSDMD-N cleaves and perforates the cell membrane, producing large amounts of LDH, IL-1β, IL-18 and HMGB1, which flow out from pores in the cell membrane to the outside of the cell, causing inflammatory responses.[13–16] The cleavage of GSDMD and the release of LDH, IL-1β, IL-18 and HMGB1 are considered as important features of pyroptosis. In the present study, the results of Western blot and immunofluorescence showed that, compared with the normal rats, the expressions of GSDMD ($P<0.0001$) and GSDMD-N ($P=0.0003$) and the percentage of the GSDMD-positive cells ($P<0.0001$) in the liver tissue of ACLF rats significantly increased (Figure 2A–E). The serum LDH level of ACLF rats was also significantly higher than that of normal rats ($P=0.0006$) (Figure 2F). The results of Western blot, ELISA and RT-qPCR suggested, that compared with the normal group, the expressions of pro-IL-1β, IL-1β and IL-18 in the liver tissue of ACLF rats significantly increased (Western blot: $P=0.0006$, $P=0.0015$, $P=0.0008$; the rest of the results: each $P<0.0001$) (Figure 2G–N). Importantly, compared with the ACLF model group, the expressions of GSDMD (Western blot: $P=0.0001$, $P=0.0008$, Figure 2A and B), GSDMD-N (Western blot: $P=0.0001$, $P<0.0001$, Figure 2A and C), IL-1β (Western blot: $P=0.0007$, $P=0.0069$, Figure 2I and K; ELISA: $P=0.0060$, $P=0.5326$, Figure 2G; RT-qPCR: $P=0.0132$, $P=0.5650$, Figure 2M) and IL-18 (Western blot: $P=0.0048$, $P=0.0138$, Figure 2I and L; ELISA: $P<0.0001$, $P=0.0173$ Figure 2H; RT-qPCR: $P=0.0053$, $P=0.0201$, Figure 2N) in the HMGB1 inhibitor group and the Caspase-1 inhibitor group significantly down-regulated, and the percentage of the GSDMD-positive cells (each $P<0.0001$) and the serum LDH level ($P=0.0196$, $P=0.0243$) significantly decreased (Figure 2D–F). These results indicated that there was obvious pyroptosis in the liver tissue of ACLF rats.

To further confirm the existence of hepatocyte pyroptosis in the liver tissue of ACLF rats and observe the degree of hepatocyte pyroptosis, we performed triple-immunostaining of active Caspase-1, TUNEL and ALB. Active Caspase-1+/TUNEL+/ALB+ triple-positive cells were considered as pyroptotic hepatocytes, and the results showed almost no triple positive cells in the normal group. On the contrary, a large number of pyroptotic hepatocytes were found in the ACLF model group, which were widely distributed in the damaged liver tissue, and the percentage of pyroptotic hepatocytes was far more than in the normal group ($P<0.0001$) (Figure 2O and P). Importantly, pre-treatment with the HMGB1 inhibitor or the Caspase-1 inhibitor prominently improved this phenomenon (each $P<0.0001$) (Figure 2O and P). These results indicated that the liver of ACLF rats showed severe hepatocyte pyroptosis, which was probably induced by high levels of HMGB1. More importantly, this is the first discovery that pyroptosis is involved in the pathogenesis of ACLF.

HMGB1 Induced Hepatocyte Pyroptosis in ACLF Rats by Activating the Caspase-1-Dependent Pyroptosis Pathways

To further study how HMGB1 and hepatocyte pyroptosis were involved in the development of ACLF, we determined the expressions of Caspase-1, cleaved Caspase-1, GSDMD, GSDMD-N, pro-IL-1β, IL-1β, and IL-18, which are key genes and proteins in the Caspase-1-dependent pyroptosis pathways. In addition, we detected the expressions of NF-κB, IL-6, TNF-α, NLRP3, and ASC, which are key genes and proteins in the upstream of the pathways. Specifically, the results of Western blot, RT-qPCR, and ELISA showed that, compared with the normal group, the expressions of NF-κB, NLRP3, ASC, IL-6 and TNF-α significantly increased in liver tissue of rats in the ACLF model group (RT-qPCR: *NLRP3:* $P=0.0001$; ELISA: IL-6: $P=0.0002$; the rest of the results: each $P<0.0001$) (Figure 3A–D and 3F–I). The activity of Caspase-1 was calculated by the ratio of cleaved Caspase-1/(Caspase-1 +cleaved Caspase-1), and the results showed that, the ratio in the ACLF model group was significantly higher than that in the normal group (the ratio: $P=0.0006$, Figure 3A and E). Importantly, pre-treatment with the HMGB1 inhibitor or the Caspase-1 inhibitor decreased the expressions of NLRP3 (Western blot: $P=0.0004$, $P=0.0344$, Figure 3A and C; RT-qPCR: $P=0.0151$, $P=0.3846$, Figure 3F),

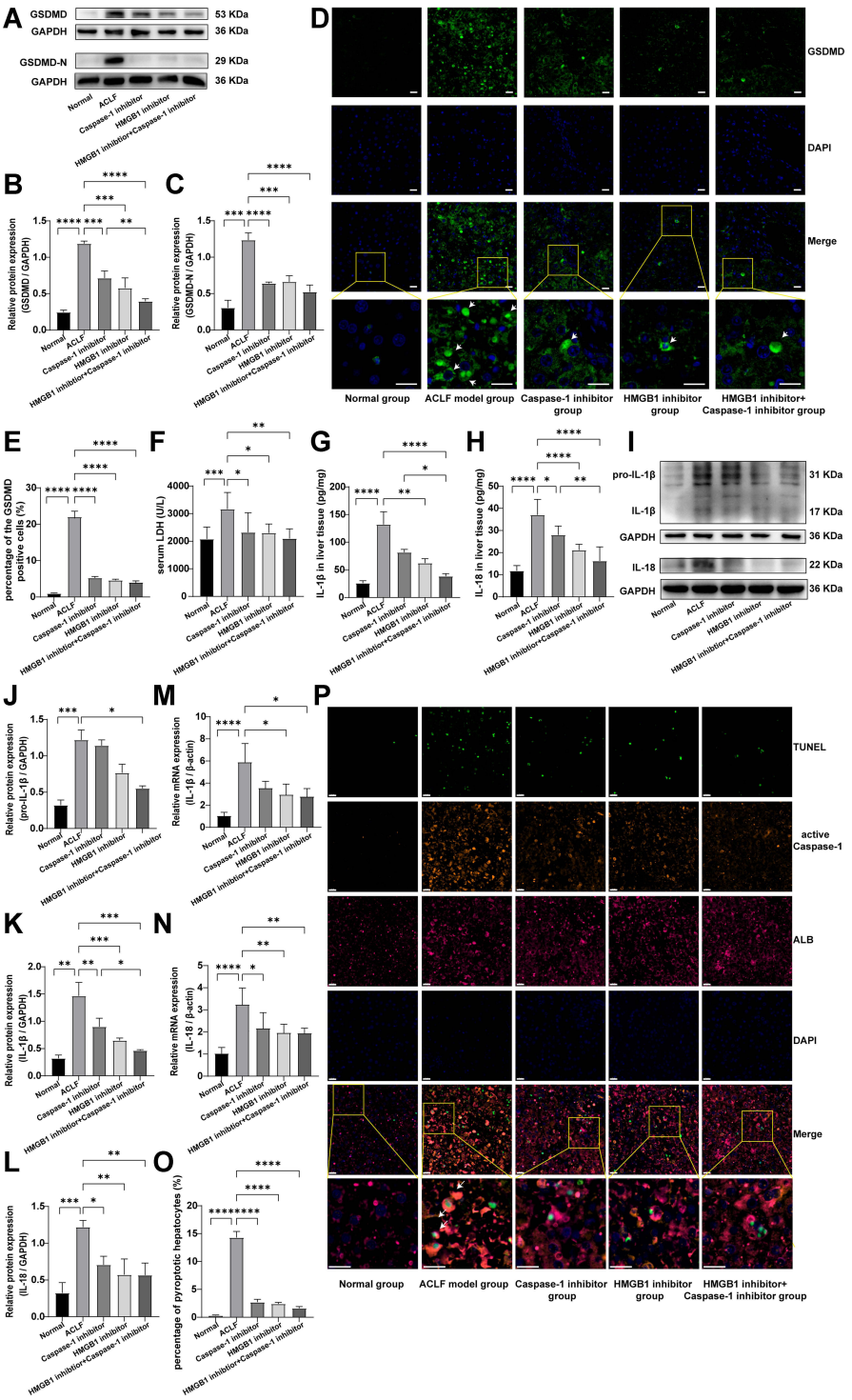

Figure 2 The livers of ACLF rats showed severe hepatocyte pyroptosis.

Notes: (**A**–**C**) The expression levels of GSDMD and GSDMD-N were detected by Western blot, and GAPDH was used as the loading control. n=3 per group. (**D** and **E**) The percentage of GSDMD-positive cells in liver tissues of rats in each group was detected by immunofluorescence (magnification, ×400; scale bar=20 μm). A region is boxed randomly in each group and the boxed regions are further enlarged (magnification, ×1200; scale bar=20 μm). The arrows represent GSDMD-positive cells. n=3 per group. (**F**) The serum LDH levels of rats in each group. The normal group (n=9), the ACLF model group (n=8), the inhibitor groups (each n=7). (**G** and **H**) ELISA was used to determine the levels of IL-1β and IL-18 in liver tissues. The normal group (n=9), the ACLF model group (n=8), the inhibitor groups (each n=7). (**I**–**L**) The expressions of pro-IL-1β, IL-1β and IL-18 were detected by Western blot, and GAPDH was used as the loading control. n=3 per group. (**M** and **N**) Relative transcript levels of *IL-1β* and *IL-18* in the different groups were detected by RT-qPCR. *β-actin* was used as internal reference. n=6 per group. (**O** and **P**) Immunofluorescence triple staining of TUNEL, active Caspase-1 and ALB was used to further investigate hepatocyte pyroptosis in ACLF rats (magnification, ×400; scale bar=20 μm). A region is boxed randomly in each group and the boxed regions are further enlarged below (magnification, ×1200; scale bar=20 μm). The arrows represent active Caspase-1+/TUNEL+/ALB+ triple-positive cells. n=3 per group. Asterisks indicate statistical significance: $P^{*}< 0.05$, $P^{**}< 0.01$, $P^{***}< 0.001$, and $P^{****}< 0.0001$.

Abbreviations: ACLF, acute-on-chronic liver failure; GSDMD, Gasdermin D; LDH, lactate dehydrogenase; ELISA, enzyme-linked immunosorbent assay; IL-1β, interleukin-1 β; IL-18, interleukin-18; RT-qPCR, quantitative real-time PCR; TUNEL, terminal deoxynucleotidyl transferase dUTP nick end labeling.

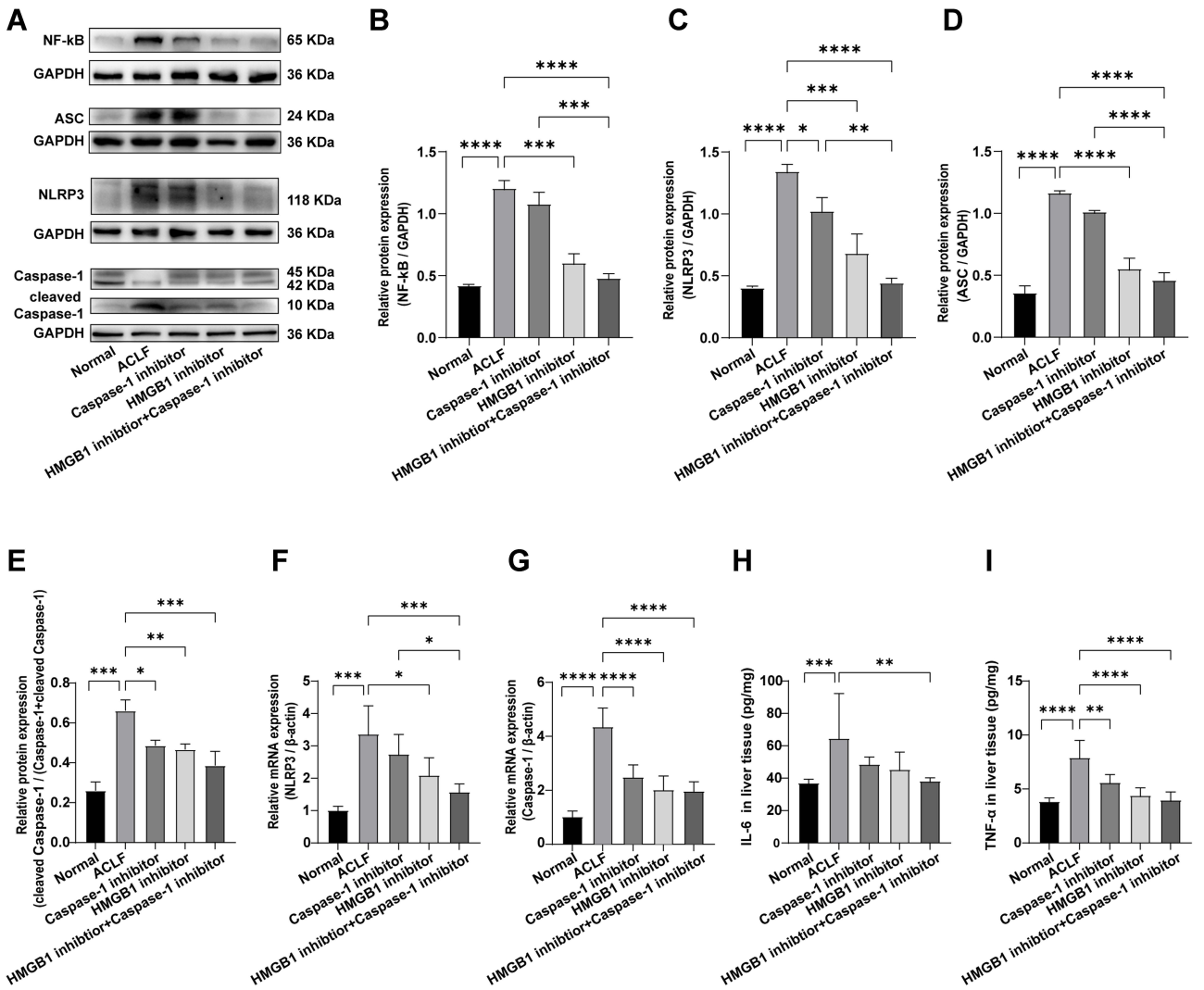

Figure 3 HMGB1 induced hepatocyte pyroptosis in ACLF rats by activating the Caspase-1-dependent pyroptosis pathways.

Notes: (**A**–**E**) The expression levels of NF-κB, NLRP3, ASC, Caspase-1 and cleaved Caspase-1 were detected by Western blot, and GAPDH was used as the loading control. n=3 per group. (**F** and **G**) Relative transcript levels of *NLRP3* and *Caspase-1* in the different groups were detected by RT-qPCR. *β-actin* was used as internal reference. n=6 per group. (**H** and **I**) ELISA was used to determine the levels of IL-6 and TNF-α in liver tissues. The normal group (n=9), the ACLF model group (n=8), the inhibitor groups (each n=7). Asterisks indicate statistical significance: *P**< 0.05, *P***< 0.01, *P****< 0.001, and *P*****< 0.0001.

Abbreviations: HMGB1, High mobility group box-1; ACLF, acute-on-chronic liver failure; ASC, the adaptor protein apoptosis-associated speck-like protein containing a caspase recruitment domain; RT-qPCR, quantitative real-time PCR; ELISA, enzyme-linked immunosorbent assay; IL-6, interleukin-6; TNF-α, tumor necrosis factor-α.

cleaved Caspase-1/(Caspase-1+cleaved Caspase-1) (Western blot: P=0.0055, P=0.0102, Figure 3A and E), Caspase-1 (RT-qPCR: each P<0.0001, Figure 3G), and TNF-α (ELISA: P<0.0001, P = 0.0036, Figure 3I). The expressions of NF-κB and ASC significantly reduced due to pre-treatment with the HMGB1 inhibitor (Western blot: P=0.0001, P<0.0001), but there were no significant differences in the Caspase-1 inhibitor group (Western blot: P=0.3265, P=0.0814) (Figure 3A, B and D). Combined with the results of GSDMD, GSDMD-N, pro-IL-1β, IL-1β and IL-18 in the pathways (Figure 2A–E and G–N), we found that inhibition of Caspase-1 alleviated the expression of genes and proteins in the Caspase-1-dependent pyroptosis pathways, and inhibiting HMGB1 reduced the expression of genes and proteins in the pathways and its upstream. These results indicated that HMGB1 induced hepatocyte pyroptosis in ACLF rats by activating the Caspase-1-dependent pyroptosis pathways.

Activation of HMGB1-Induced Hepatocyte Pyroptosis Aggravated the Inflammatory Responses and Damage of Livers in ACLF Rats

To further study the role of HMGB1 and hepatocyte pyroptosis in ACLF, we observed the pathological damage of ACLF rats by HE and MT staining, and the ultrastructural

changes in hepatocytes by TEM. The results of HE staining showed that, in the normal group, the structure of liver lobule was clear and complete, hepatocytes were orderly arranged, and there was no cell degeneration or necrosis. In the ACLF model group, liver fibrosis was obvious, pseudolobules were widely formed, hepatocytes were disordered, and necrosis was severe and accompanied by a large number of inflammatory cell infiltration, hepatic sinusoidal dilation and hemorrhage, with some liver tissues showing massive or submassive necrosis. ACLF rats pre-treated with the Caspase-1 inhibitor or the HMGB1 inhibitor showed liver fibrosis, apparent formation of pseudolobules in the livers, inflammatory cell infiltration, and different degrees of liver tissue necrosis, but the degree of necrosis was lower than that of ACLF model group, and the latter had less severe liver damage (Figure 4A). The results of MT staining showed that the morphology and structure of liver lobules and portal areas in the normal group were intact, and hepatic cords were radially arranged. There was significant hyperplasia of collagen fibers in most portal areas of the ACLF rats, and it was obvious that some portal areas were bridged by hyperplastic collagen fibers. The structure of liver lobules was destroyed, pseudolobules were widely formed, and liver fibrosis and cirrhosis were obvious. There was no significant difference in the degree of liver fibrosis between the inhibitor groups and the ACLF model group (Figure 4B). The results of TEM showed that the structure of liver cells in the normal group was intact and the nuclei were large and round. The endoplasmic reticulum (ER) was well developed and neatly arranged in the cytoplasm. The mitochondria, which were mostly spherical or ellipsoid, were abundant and evenly distributed, the crests were well developed, and the bilayer membrane structure was complete. The lysosomes were monolayers and appeared black under TEM. In the ACLF model group, the nuclei were deformed and condensed, the ER was dilated or even fractured, the mitochondria appeared swollen, the membranes were ruptured, the stromata were hollow, the cristae were fractured or disappearing, and the lysosomal membranes were ruptured and released some substances. The degree of hepatocyte damage in the inhibitor groups was mild, the nuclei were slightly deformed, the ER was dilated but the structure was still intact, the mitochondria were swollen and deformed but the crests were clear, membranes rupture was mild, and the lysosomal membrane was intact (Figure 4C). In addition, we measured the liver function and the coagulation function in each group, and the results showed that, compared with normal rats, the serum levels of ALT, AST and TBIL in ACLF rats significantly increased (each $P<0.0001$) (Figure 5A–C), ALB decreased ($P=0.0019$) (Figure 5D), the PT was prolonged, and the INR increased (each $P<0.0001$) (Figure 5E and F). Interestingly, pre-treatment with the HMGB1 inhibitor or the Caspase-1 inhibitor significantly reduced the levels of ALT ($P<0.0001$, $P=0.0001$) and AST (each $P<0.0001$) in ACLF rats (Figure 5A and B). Furthermore, the HMGB1 inhibitor significantly shortened the PT and reduced the INR (each $P=0.0023$) (Figure 5E and F). These results indicated that ACLF rats suffered severe liver pathological damage, liver dysfunction and coagulation disorder. The inhibition of HMGB1 and Caspase-1 prominently improved the liver function and pathological damage in ACLF rats, and the inhibition of HMGB1 further improved the coagulation function in ACLF rats.

The liver damage in ACLF rats was associated with the inflammatory response, which was further confirmed by the levels of IL-6, TNF-α, IL-1β and IL-18, and the results of HE staining (Figures 3H, I, 2G–N and 4A). The process of pyroptosis is accompanied by the production and release of inflammatory cytokines such as IL-6, TNF-α, IL-1β and IL-18, which induce the immune cascade to expand local and systemic inflammatory reactions and ultimately aggravate tissue damage. These results indicated that the activation of HMGB1-induced hepatocyte pyroptosis resulted in inflammatory responses, which caused liver dysfunction, coagulation disorder and severe liver damage in ACLF rats. HMGB1-induced hepatocyte pyroptosis expanded inflammatory responses to aggravate ACLF.

Dual Inhibition of HMGB1 and Caspase-1 Attenuated HMGB1-Induced Hepatocyte Pyroptosis and Inflammatory Responses in ACLF Rats

To further confirm that HMGB1-induced hepatocyte pyroptosis expanded the inflammatory responses to aggravate ACLF, we investigated whether the dual inhibition of HMGB1 and Caspase-1 can further regulate the activation of HMGB1, hepatocyte pyroptosis, inflammatory responses and tissue damage in ACLF rats. The results of Western blot showed that, compared with the ACLF model group, the expression of HMGB1 significantly increased in the cell nucleus and decreased in the cytoplasm in the HMGB1 inhibitor+Caspase-1 inhibitor group ($P=0.0355$; $P<0.0001$), with the dual inhibition significantly attenuating the phenomenon of

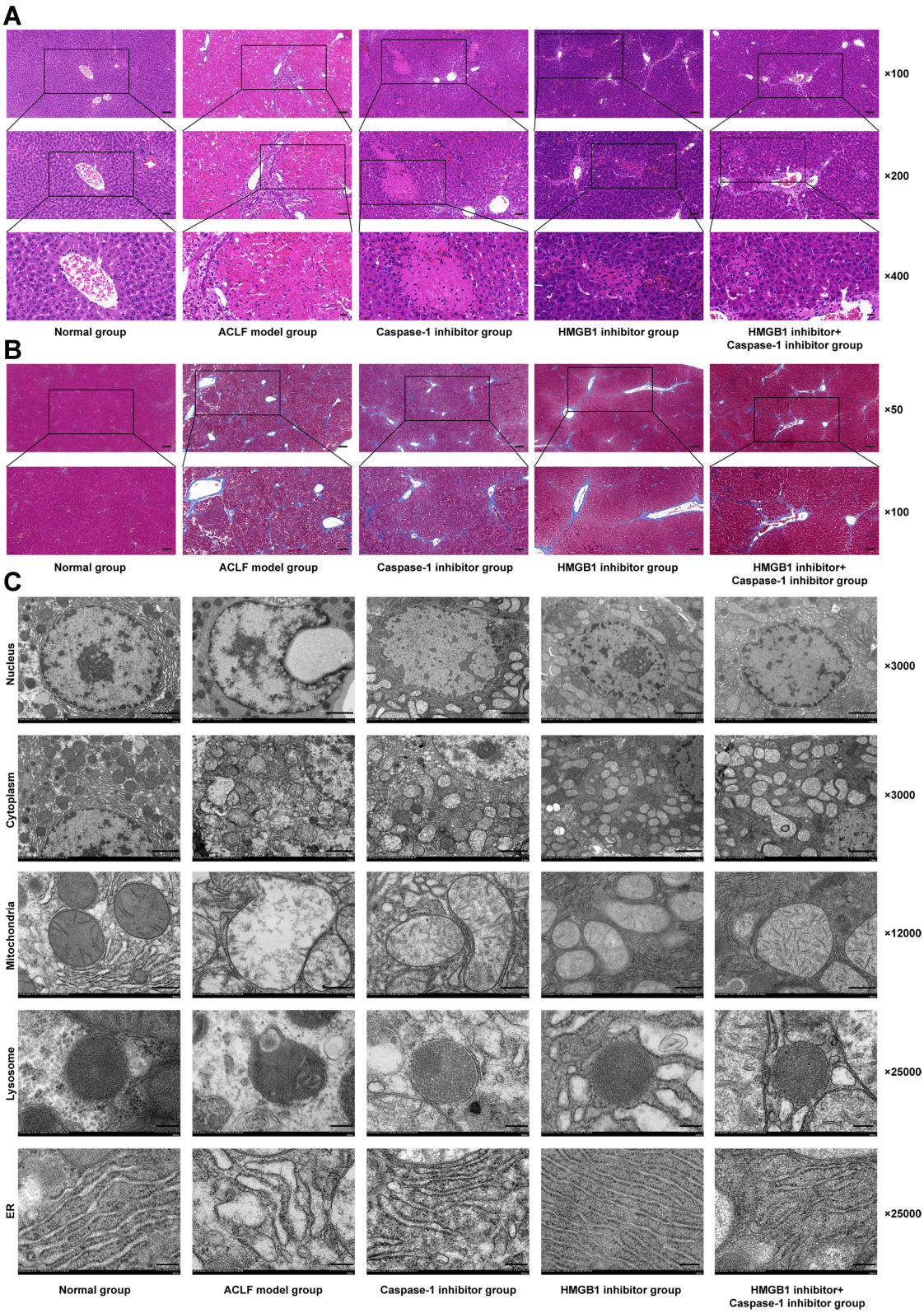

Figure 4 Pathological damage of liver tissue in each group.

Notes: (**A**) HE staining of hepatic tissues from the different groups (magnification, ×100, ×200, and ×400; scale bar=100, 50, and 20 μm); (**B**) MT staining of hepatic tissues from the different groups (magnification, ×50 and ×100; scale bar=200 and 100 μm); (**C**) TEM was used to examine the ultrastructural changes of hepatocytes, including the hepatocyte nucleus, cytoplasm, mitochondria, lysosome, and ER (magnification, ×3000, ×3000, ×12,000, ×25,000, and ×25,000; scale bar=2 μm, 2 μm, 500 nm, 200 nm, and 200 nm).

Abbreviations: HE staining, hematoxylin and eosin staining; MT staining, masson's trichrome staining; TEM, transmission electron microscopy; ER, endoplasmic reticulum.

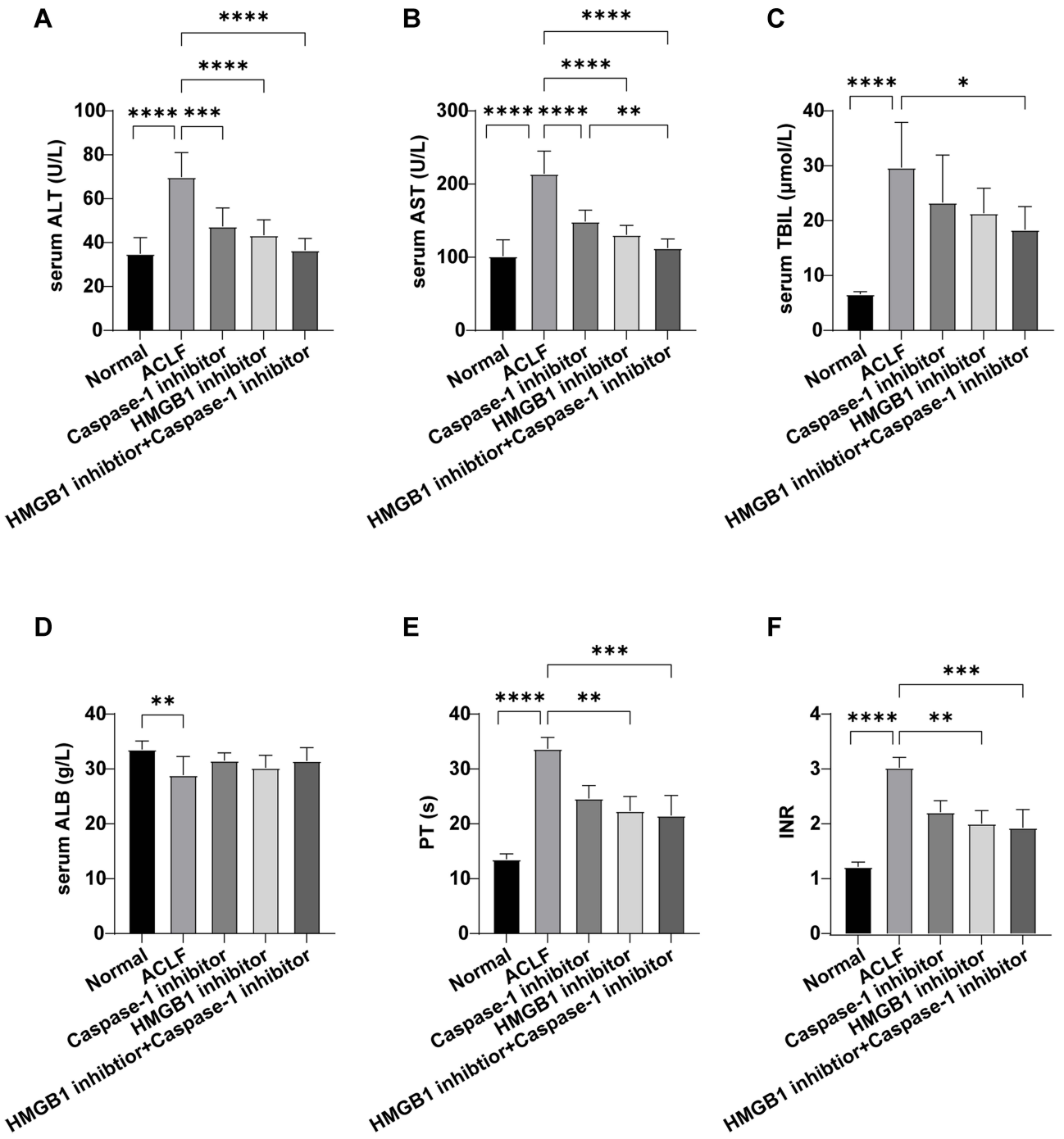

Figure 5 Liver function and coagulation function of rats in each group.
Notes: (**A**) Serum ALT level; (**B**) Serum AST level; (**C**) Serum TBIL level; (**D**) Serum ALB level; (**E**) PT in each group; (**F**) INR in each group. The normal group (n=9), the ACLF model group (n=8), the inhibitor groups (each n=7). Asterisks indicate statistical significance: *P**< 0.05, *P***< 0.01, *P****< 0.001, and *P*****< 0.0001.
Abbreviations: ALT, alanine aminotransferase; AST, aspartate aminotransferase; TBIL, total bilirubin; ALB, albumin; PT, prothrombin time; INR, international normalized ratio.

translocation from the nucleus to the cytoplasm; and the expression of HMGB1 in the cytoplasm of the HMGB1 inhibitor+Caspase-1 inhibitor group was lower than that of the Caspase-1 inhibitor group (*P*=0.0025) (Figure 1A–C); immunofluorescence results also confirmed this phenomenon (Figure 1D). The transcript level of *HMGB1* in liver tissue of the HMGB1 inhibitor +Caspase-1 inhibitor group, the serum HMGB1 level and the levels of TLR4 and RAGE in the liver tissue and serum were lower than those of the ACLF model

group (the transcript level of *HMGB1:* P=0.0005, the rest of the results: each P<0.0001) (Figure 1E–K). And the effect of reducing TLR4 and the serum HMGB1 level was stronger than in each of the HMGB1 inhibitor group and the Caspase-1 inhibitor group (Western blot result of TLR4: P=0.0336, P<0.0001; ELISA result of TLR4: P=0.0002, P<0.0001; ELISA result of HMGB1: P=0.0003, P<0.0001), the effect of reducing RAGE was stronger than in the Caspase-1 inhibitor group (Western blot: P<0.0001; ELISA: P=0.0143). These results suggested that dual inhibition of HMGB1 and Caspase-1 further reduced the activation of HMGB1, and the effect was stronger than the effect of inhibition of only Caspase-1.

We found that, compared with the ACLF model group, the protein expressions of NF-κB (Western blot: P<0.0001, Figure 3A and B), NLRP3 (Western blot: P<0.0001, Figure 3A and C), ASC (Western blot: P<0.0001, Figure 3A and D), cleaved Caspase-1/(Caspase-1+cleaved Caspase-1) (Western blot: P=0.0006, Figure 3A and E), GSDMD (Western blot: P<0.0001, Figure 2A and B; immunofluorescence: P<0.0001, Figure 2D and E), GSDMD-N (Western blot: P<0.0001, Figure 2A and C), pro-IL-1β (Western blot: P=0.0395, Figure 2I and J; ELISA: P<0.0001, Figure 2G), IL-1β (Western blot: P=0.0002, Figure 2I and K), IL-18 (Western blot: P=0.0048, Figure 2I and L; ELISA: P<0.0001, Figure 2H), IL-6 (ELISA: P=0.0088, Figure 3H), and TNF-α (ELISA: P<0.0001, Figure 3I) in the liver tissue of rats, and the serum LDH levels (P=0.0034, Figure 2F) significantly decreased in the HMGB1 inhibitor+Caspase-1 inhibitor group, the transcript levels of *NLRP3, Caspase-1, IL-1β* and *IL-18* reduced (P=0.0007, P<0.0001, P=0.0115, P=0.0048) (Figures 3F, G and 2M, N). The percentage of the active Caspase-1+/TUNEL+/ALT triple-positive cells with double inhibition in the HMGB1 inhibitor+Caspase-1 inhibitor group was lower than in the ACLF model group (P<0.0001) (Figure 2O and P). The expressions of NF-κB (Western blot: P=0.0001, Figure 3A and B), NLRP3 (Western blot: P=0.0011, Figure 3A and C; RT-qPCR: P=0.0279, Figure 3G), ASC (Western blot: P<0.0001, Figure 3A and D), GSDMD (Western blot: P=0.0098, Figure 2A and B), IL-1β (Western blot: P=0.0280, Figure 2I and K; ELISA: P=0.0126, Figure 2G) and IL-18 (ELISA: P=0.0022, Figure 2H) in the liver tissue of the HMGB1 inhibitor +Caspase-1 inhibitor group were significantly lower than in the liver tissue of the Caspase-1 inhibitor group. The data showed that the dual inhibition of HMGB1 and Caspase-1 further alleviated HMGB1-induced hepatocyte pyroptosis, with the effect stronger than the effect of inhibition of only Caspase-1 inhibitor group. These results indicated that HMGB1 induced hepatocyte pyroptosis in ACLF rats by activating the Caspase-1-dependent pyroptosis pathways.

Liver inflammation, liver dysfunction, coagulation disorder and pathological damage of ACLF rats prominently improved in the HMGB1+Caspase-1 inhibitor group. Specifically, compared with the ACLF model group, the levels of serum ALT, AST and TBIL in the HMGB1 inhibitor +Caspase-1 inhibitor group significantly decreased (P<0.0001, P<0.0001, P=0.0121, Figure 5A–C), the PT shortened, and the INR decreased (each P=0.0007, Figure 5E and F). The effect of reduction of AST (P=0.0073, Figure 5B) in the HMGB1 inhibitor +Caspase-1 inhibitor group was stronger than in the Caspase-1 inhibitor group. HE staining results showed that the degree of hepatocyte necrosis, inflammatory cell infiltration and pathological damage of liver was lower in the dual inhibitor group than in each of the ACLF model group, the HMGB1 inhibitor group and the Caspase-1 inhibitor group (Figure 4A). The results of TEM showed that the degree of ultrastructural damage of hepatocytes in the dual inhibitor group was lower than in the ACLF model group (Figure 4C). Therefore, together with the results of the inflammatory factors IL-6, TNF-α, pro-IL-1β, IL-1β and IL-18 (Figures 3I and J and 2G–N), the data suggested that the dual inhibition of HMGB1 and Caspase-1 improved liver function, coagulation function and pathological damage, and reduced liver inflammatory responses, with the effect stronger than the effect of inhibition of only Caspase-1.

In summary, the dual inhibition of HMGB1 and Caspase-1 regulated the activation of HMGB1, hepatocyte pyroptosis, inflammatory responses, liver function, coagulation function and pathological damage. These results suggested that HMGB1-induced hepatocyte pyroptosis expanded inflammatory responses to aggravate ACLF.

Discussion

This study reveals, for the first time, that pyroptosis is a key pathophysiological event of ACLF and is involved in the pathogenesis of ACLF, and that high levels of HMGB1 activate Caspase-1-dependent pyroptosis by combining with TLR4 and RAGE, thus expanding liver inflammatory responses and causing pathological damage, and eventually developed into ACLF. This unprecedented discovery provides new clues to the pathogenesis of ACLF, and may be exploited more effective ways for the

evaluation, diagnosis, and treatment of this difficult and complicated disease.

ACLF is a kind of innate immune dysfunction syndrome. ACLF patients often present with pro-inflammatory states, such as local liver inflammation and systemic inflammatory response syndrome (SIRS), and are plagued by immunosuppression, which presents as acquired immunodeficiency, resulting in liver failure manifestations such as coagulation dysfunction and severe decompensation in liver function; they are also highly susceptible to multiple complications such as infection and ascites which may develop into multiple organ failure.[24] Thus, immune dysfunction and inflammatory responses are central to the progression of ACLF.[4,5] HMGB1, as a DAMP, activates immune cells by binding to its receptor RAGE or TLR4, thereby transforming the cells into pro-inflammatory phenotypes, initiating inflammatory signals through the release of cytokines and chemokines, and amplifying and maintaining the inflammatory responses.[7,24] Studies have shown that when exogenous microorganisms invade or endogenous tissue damage occurs, HMGB1 is released to the outside of the cell in two ways: as stress signal and inflammatory mediators, where one is actively secreted to the outside of the cell by activated macrophages, monocytes and dendritic cells, and the other is passively released from necrotic cells to the outside of the cell.[24,25] Macrophages are one of the most important innate immune cells to fight infection. Hepatic macrophages are also known as kupffer cells (KC), which account for more than 80% of human macrophages. KC participates in liver immune responses through phagocytosis, antigen presentation and production of various cytokines and chemokines, causing inflammation, necrosis and fibrosis.[26] In the process of liver damage such as ACLF and acute liver failure (ALF), the immune system responds to invading pathogens and damaged liver tissue by recognizing pathogen-related molecular patterns (PAMPs) (such as LPS, etc.) and DAMPs (such as HMGB1, IL-1, ATP, etc.). Both PAMPs and DAMPs interact with pattern recognition receptors (PRRs) on macrophages to activate macrophages, and the activated macrophages secrete pro-inflammatory factors such as HMGB1 and release them outside the cell,[24] thus triggering the inflammatory response. Once HMGB1 translocates to the outside of the cell membrane, its binds with its receptor RAGE or TLR4 to initiate pyroptosis as a DAMP molecule[10–12] and trigger inflammatory responses. A study found that the serum HMGB1 level of patients with chronic hepatitis B virus-related ACLF (HBV-ACLF) was significantly higher than that of healthy people and chronic hepatitis B (CHB) patients.[27] There was no phenomenon of HMGB1 translocation from the nucleus to the cytoplasm in the liver cells of healthy people and CHB patients, but it was obviously present in ACLF patients.[28] Consistent with previous reports, in our study, HMGB1 showed obvious translocation from the nucleus to the cytoplasm in ACLF rats, and the expression levels of HMGB1, TLR4 and RAGE significantly increased in the liver tissue and serum. These results suggested that HMGB1 was activated in the liver tissue of ACLF rats. To further demonstrate that the development of ACLF was associated with the upregulation and translocation of HMGB1, we employed HMGB1 inhibition, Caspase-1 inhibition and dual inhibition of HMGB1 and Caspase-1 in this study. Interestingly, both HMGB1 inhibition and dual inhibition significantly downregulated the levels of HMGB1, TLR4 and RAGE in the liver tissue and serum and reduced translocation of HMGB1, but the combined inhibition effect was more significant. In addition, Caspase-1 inhibition downregulated the expression and release of RAGE, and inhibited the expression of HMGB1 in the cytoplasm. These results strongly suggested that HMGB1 was activated in the liver tissue of ACLF rats and was involved in the progression of ACLF. Inhibition of HMGB1 prominently ameliorated this phenomenon, with the combined inhibition effect much stronger.

Considering that the activation of HMGB1 is closely related to pyroptosis, we further investigated whether pyroptosis occurred in liver tissue of ACLF rats. The expressions of GSDMD, GSDMD-N, pro-IL-1β, IL-1β, IL-18 and the percentage of the GSDMD-positive cells in the liver tissue of ACLF rats significantly increased. The serum LDH level of ACLF rats was also significantly higher than that of normal rats. Importantly, pre-treatment with the HMGB1 inhibitor or the Caspase-1 inhibitor, or dual inhibition of Caspase-1 and HMGB1, significantly improved this phenomenon. The dual inhibition effect was most significant for these reductions. These results indicated that there was significant pyroptosis in the liver tissue of ACLF rats. In addition, a large number of pyroptotic hepatocytes were found in the ACLF model group, widely distributed in the damaged liver tissue. Importantly, pre-treatment with the HMGB1 inhibitor or the Caspase-1 inhibitor, or dual inhibition, prominently improved this phenomenon, with the dual inhibition the

most effective. Our data indicate, for the first time, that the livers of ACLF rats show severe pyroptosis, that pyroptosis is involved in the pathogenesis of ACLF, which in turn is related to the activation of HMGB1, and that the inhibition of HMGB1 significantly ameliorates the levels of the parameters related to pyroptosis, with dual inhibition of HMGB1 and Caspasce-1 revealing a stronger effect of anti-pyroptosis.

So how does HMGB1 induce pyroptosis? After HMGB1 is released outside the cell, it activates the myeloid differentiation factor 88 (MyD88)-dependent TLR4 signaling pathway and enhances the expression of NF-κB by binding to TLR4.[29] The NF-κB-mediated inflammatory cascade releases pro-inflammatory factors such as IL-1β, IL-18, IL-6, and TNF-α, induces the activation of NLRP3 inflammasomes, and stimulates the intracellular pattern-recognition receptors (PRRs) to recognize these signals. NLRP3 combines with ASC and Caspase-1 to form a multi-protein complex that promotes self-cleavage of Caspase-1 to form active cleaved Caspase-1.[30,31] On one hand, the cleaved Caspase-1 cuts GSDMD to form a peptide containing the N-terminal domain, namely GSDMD-N, leading to perforation of cell membranes, increase in cell permeability, and release of intracellular substances such as HMGB1 and LDH, which result in pyroptosis and expansion of the inflammatory responses.[32–34] On the other hand, the cleaved Caspase-1 cleaves pro-IL-1β and pro-IL-18 to form active IL-1β and IL-18, which are released to the outside of the cell, and recruits inflammatory cells to aggregate, causing pyroptosis and expanding and maintaining the inflammatory responses.[35] These processes give rise to two Caspase-1-dependent pyroptosis pathways. In line with previous reports, we found the expressions of key genes and proteins in the Caspase-1-dependent pyroptosis pathways (cleaved Caspase-1, GSDMD, GSDMD-N, pro-IL-1β, IL-1β and IL-18) and its upstream (NF-κB, IL-6, TNF-α, NLRP3, and ASC) of the ACLF model group significantly increased. Importantly, the expressions of proteins and genes in the pathways decreased pre-treated with the HMGB1 inhibitor, the Caspase-1 inhibitor or both the HMGB1 and Caspase-1 inhibitors. The expressions of genes and proteins in the upstream of the pathways significantly reduced in the HMGB1 inhibitor group and the HMGB1 inhibitor+Caspase-1 inhibitor group. RAGE is a transmembrane receptor whose activation plays an important role in mediating pro-inflammatory responses.[25] HMGB1 interacts with RAGE to increase the permeability and rupture of the lysosome membrane, activate and release cathepsin B,[8] which directly activates NLRP3 through the leucine-rich repeat (LRR) domain of NLRP3,[36,37] and induce pyroptosis through downstream Caspase-1-dependent pyroptosis pathways. In addition, HMGB1 in combination with RAGE activates NF-κB to produce a variety of pro-inflammatory cytokines, and activates IL-1β and IL-18 by cleaving and activating pro-IL-1β and pro-IL-18, thereby inducing pyroptosis.[38] We observed, using TEM, that the lysosomal membranes ruptured and released some substances in the ACLF model group, but remained intact in the inhibitor groups. Our data showed that HMGB1 aggravated ACLF in rats by inducing Caspase-1-dependent hepatocyte pyroptosis, and the inhibition of HMGB1 significantly reduced the levels of parameters related to pyroptosis in Caspase-1-dependent pyroptosis pathways and also reduced inflammation of ACLF, and the dual inhibition of HMGB1 and Caspase-1 showed a stronger effect.

Pyroptotic cells form pores in the cell membrane to destroy the integrity of the cell membrane, which leads to the imbalance of substances inside and outside the cell and the release of intracellular substances that induce and aggravate the inflammatory responses.[39] At the same time, inflammatory factors such as IL-1β and IL-18 released during the process of pyroptosis recruit more inflammatory cells and expand the inflammatory responses.[40] It has been reported that GSDMD-mediated hepatocyte pyroptosis expanded inflammatory responses, leading to ALF, by upregulating monocyte chemotactic protein 1/CC chemokine receptor-2 to recruit macrophages.[14] In the present study, we found that the expressions of IL-6, TNF-α, IL-1β and IL-18 were significantly higher in the liver tissues of ACLF rats than in the liver tissues of normal rats. Interestingly, HMGB1 inhibition, Caspase-1 inhibition or dual inhibition of HMGB1 and Caspase-1 significantly ameliorated this phenomenon, and the dual inhibition had a stronger effect of anti-inflammation. HE and MT staining results showed that in the ACLF model group, liver fibrosis was obvious, pseudolobules were widely formed, hepatocytes were disordered, and necrosis was severe, and accompanied by a large number of inflammatory cells infiltration, hepatic sinusoidal dilation and hemorrhage, with some liver tissues showing massive or submassive necrosis. ACLF rats pretreated with the Caspase-1 inhibitor, the HMGB1 inhibitor, or both the Caspace-1 and HMGB1 inhibitors showed inflammatory cell infiltration and the degree of necrosis was lower in all three than in the ACLF model group,

with the dual inhibition showing the least damage. There was no significant difference in the degree of liver fibrosis between the inhibitor groups and the ACLF model group. The results of TEM showed that the nuclei of the ACLF model group were deformed and condensed, the ER was dilated or even fractured, the mitochondria appeared swollen, the membranes were ruptured, the stromata were hollow, the cristae were fractured or disappearing, and the lysosomal membranes were ruptured and released some substances. The hepatocyte damage in the inhibitor groups was mild, the nuclei were slightly deformed, the ER was dilated but the structure was still intact, the mitochondria were swollen and deformed but the crests were clear, the membrane rupture was slight with the lysosomal membrane still intact. In addition, in the ACLF rats, serum ALT, AST and TBIL levels significantly increased, ALB decreased, the PT was prolonged, and the INR increased. These indicated severe liver damage, liver dysfunction and coagulation disorder in ACLF rats. Importantly, liver function and coagulation function were significantly improved due to pre-treatment with the HMGB1 inhibitor, the Caspase-1 inhibitor or both HMGB1 and Caspase-1 inhibitors, with the dual inhibition effect stronger. Our data indicated that HMGB1-induced hepatocyte pyroptosis aggravated inflammatory responses and pathological damage to lead to ACLF, which was improved by inhibiting HMGB1 and Caspase-1, with the dual inhibition effect stronger. The schematic diagram of HMGB1-induced hepatocyte pyroptosis pathways and their relationship with ACLF is shown in Figure 6.

Taken together, our data provide novel evidence that HMGB1-induced hepatocyte pyroptosis plays a critical role in the pathophysiology of ACLF. Our results showed that high levels of HMGB1 triggered Caspase-1-dependent pyroptosis pathways by binding with TLR4 and RAGE,

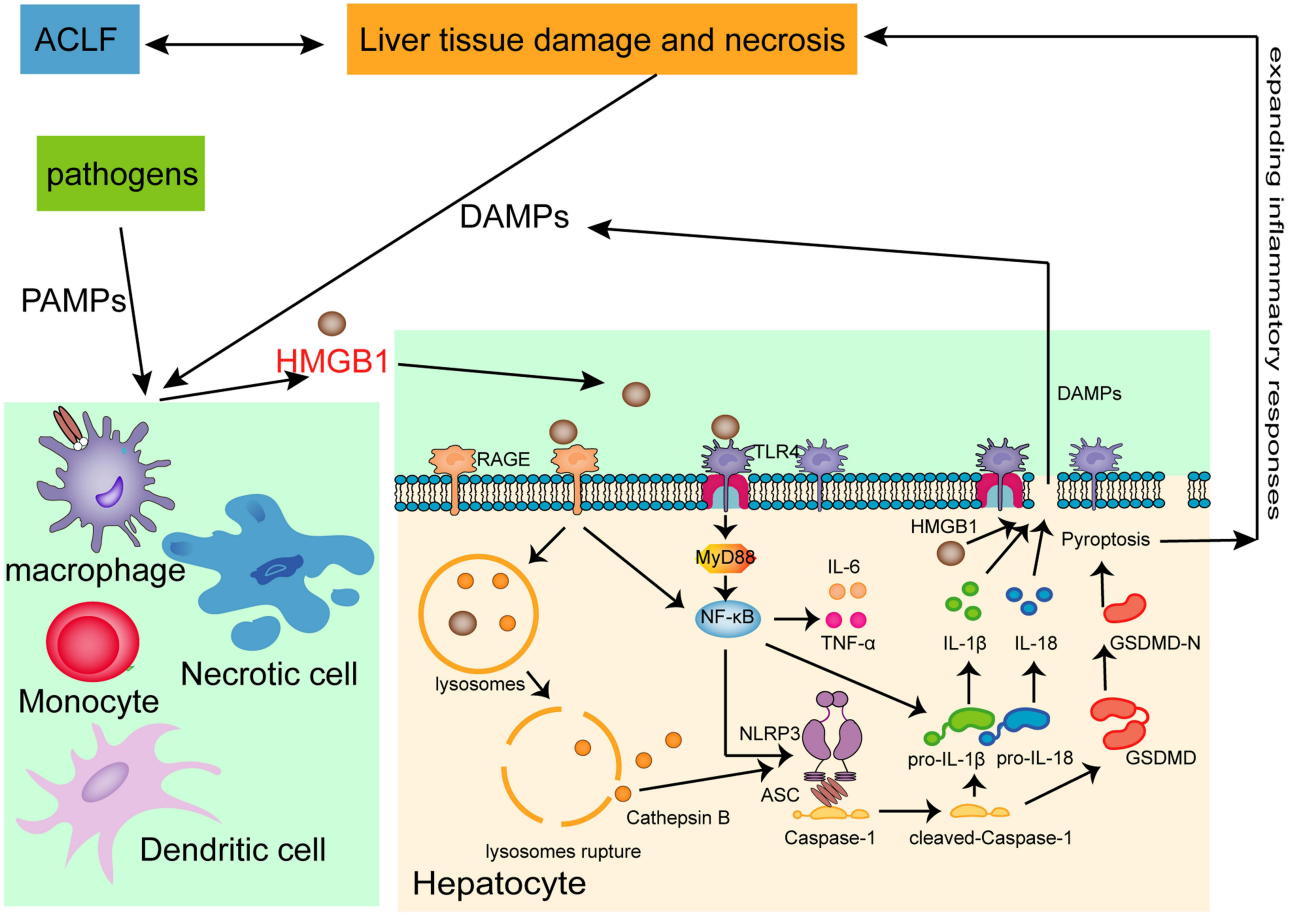

Figure 6 Schematic diagram of HMGB1-induced hepatocyte pyroptosis pathways and their relationship with ACLF.
Abbreviations: ACLF, acute-on-chronic liver failure; PAMPs, Pathogen-associated molecular patterns; DAMPs, Damage-associated molecular patterns; HMGB1, High mobility group box-1; RAGE, receptor for advanced glycation end-products; TLR4, Toll-like receptor 4; MyD88, myeloid differentiation factor 88; IL-6, interleukin-6; TNF-α, tumor necrosis factor-α; ASC, the adaptor protein apoptosis-associated speck-like protein containing a caspase recruitment domain; IL-1β, interleukin-1 β; IL-18, interleukin-18; GSDMD, Gasdermin D.

thereby inducing hepatocyte pyroptosis. Due to the sinusoidal structural characteristics of liver regional immunity, the release of DAMP molecules (such as HMGB1) from pyroptotic hepatocyte activated KC, and the pro-inflammatory factor such as HMGB1 released by activated KC could triggered hepatocyte pyroptosis, forming a feedback loop, which stimulated the immune cascade through the HMGB1-induced hepatocyte pyroptosis signaling pathways to amplify and maintain the inflammatory responses, and causally contributing to liver dysfunction, coagulation disorder, tissue damage and eventually developing into ACLF. Inhibition of HMGB1 could prominently improve this phenomenon, and the dual inhibition of HMGB1 and Caspace-1 showed a stronger effect. Our new findings suggest that HMGB1-induced hepatocyte pyroptosis is a potential and valuable therapeutic target for the treatment of ACLF.

Conclusions

In summary, our data demonstrate, for the first time, that pyroptosis is a crucial pathophysiological event of ACLF and involved in the pathogenesis of ACLF. HMGB1 activates Caspase-1-dependent pyroptosis pathways, which expands inflammatory responses, leading to liver and coagulation dysfunction and severe liver tissue damage that eventually develop into ACLF. Inhibition of HMGB1 reduces the inflammatory responses and improves pathological damage of ACLF rats by downregulating Caspase-1-dependent hepatocyte pyroptosis, and the dual inhibition of HMGB1 and Caspase-1 has a stronger effect. This unprecedented and exciting discovery provides new clues to the pathogenesis of ACLF, and may be exploit more effective ways of evaluation, diagnosis, and treatment of this difficult and complicated disease.

Ethical Approval

The study was approved by the Animal Ethics Committee of the Capital Medical University (approval ID: AEEI-2019-067), and all animal experiments were performed in accordance with the Guide for the Care and Use of Laboratory Animals of the Beijing Municipal Government.

Acknowledgments

This research was supported by the National Natural Science Foundation of China [grant number 82074237], Beijing Municipal Natural Science Foundation [grant number 7192024] and the National Key Research and Development Program of China – Research on Inheritance and Innovation of Experience (Integration of Tao and Shu) of Illustrious Senior Traditional Chinese Medicine Practitioners by adopting Multiple Research Methods [grant number 2018YFC1704100] and its subproject-Research on the Academic Viewpoints, Unique Diagnostic and Treatment Methods and Major Diseases Prevention and Treatment Experience of Illustrious Senior Traditional Chinese Medicine Practitioners in Eastern China [grant number 2018YFC1704102].

We are very grateful to Dr. Weina Hou (Postdoctoral researcher, center for research in agricultural genomics (CRAG), Barcelona, Spain) for providing language assistance, including writing assistance, organization, reading, correction and vetting of the manuscript.

Disclosure

The authors declare no conflicts of interest in relation to this work.

References

1. Xue R, Zhu X, Jia L, et al. Mitofusin2, a rising star in acute-on-chronic liver failure, triggers macroautophagy via the mTOR signalling pathway. *J Cell Mol Med*. 2019;23(11):7810–7818. doi:10.1111/jcmm.14658
2. Liver Failure and Artificial Liver Group, Chinese Society of Infectious Diseases, Chinese Medical Association, Severe Liver Disease and Artificial Liver Group, Chinese Society of Hepatology, Chinese Medical Association. [Guideline for diagnosis and treatment of liver failure (2018)]. *Chin J Clin Hepatol*. 2019;35(1):38–44. Chinese. doi:10.3969/j.issn.1001-5256
3. Hou W, Hao Y, Yang W, et al. The Jieduan-Niwan (JDNW) formula ameliorates hepatocyte apoptosis: a study of the inhibition of E2F1-mediated apoptosis signaling pathways in acute-on-chronic liver failure (ACLF) using rats. *Drug Des Devel Ther*. 2021; Volume 15:3845–3862. doi:10.2147/DDDT.S308713
4. Martin-Mateos R, Alvarez-Mon M, Albillos A. Dysfunctional immune response in acute-on-chronic liver failure: it takes two to tango. *Front Immunol*. 2019;10:973. doi:10.3389/fimmu.2019.00973
5. Moreau R. The pathogenesis of ACLF: the inflammatory response and immune function. *Semin Liver Dis*. 2016;36(2):133–140. doi:10.1055/s-0036-1583199
6. Tang Y, Zhao X, Antoine D, et al. Regulation of post-translational modifications of HMGB1 during immune responses. *Antioxid Redox Signal*. 2016;24(12):620–634. doi:10.1089/ars.2015.6409
7. Xu J, Jiang Y, Wang J, et al. Macrophage endocytosis of high-mobility group box 1 triggers pyroptosis. *Cell Death Differ*. 2014;21(8):1229–1239. doi:10.1038/cdd.2014.40
8. Xu H, Li H, Qu Y, Zheng J, Lu J. High mobility group box 1 release from cholangiocytes in patients with acute-on-chronic liver failure. *Exp Ther Med*. 2014;8(4):1178–1184. doi:10.3892/etm.2014.1904
9. Hu Y, Hu D, Fu R. Correlation between high mobility group box-1 protein and chronic hepatitis B infection with severe hepatitis B and acute-on-chronic liver failure: a meta-analysis. *Minerva Med*. 2017;108(3):268–276. doi:10.23736/S0026-4806.16.04865-5
10. Dong W, Zhu Q, Yang B, et al. Polychlorinated biphenyl quinone induces Caspase 1-mediated pyroptosis through induction of pro-inflammatory HMGB1-TLR4-NLRP3-GSDMD Signal Axis. *Chem Res Toxicol*. 2019;32(6):1051–1057. doi:10.1021/acs.chemrestox.8b00376

11. Sun Z, Nyanzu M, Yang S, et al. VX765 attenuates pyroptosis and HMGB1/TLR4/NF-κB pathways to improve functional outcomes in TBI mice. *Oxid Med Cell Longev*. 2020;2020:7879629. doi:10.1155/2020/7879629
12. Jia C, Zhang J, Chen H, et al. Endothelial cell pyroptosis plays an important role in Kawasaki disease via HMGB1/RAGE/cathespin B signaling pathway and NLRP3 inflammasome activation. *Cell Death Dis*. 2019;10(10):778. doi:10.1038/s41419-019-2021-3
13. Hu X, Chen H, Xu H, et al. Role of pyroptosis in traumatic brain and spinal cord injuries. *Int J Biol Sci*. 2020;16(12):2042–2050. doi:10.7150/ijbs.45467
14. Li H, Zhao X, Cheng Y, et al. Gasdermin D-mediated hepatocyte pyroptosis expands inflammatory responses that aggravate acute liver failure by upregulating monocyte chemotactic protein 1/CC chemokine receptor-2 to recruit macrophages. *World J Gastroenterol*. 2019;25(44):6527–6540. doi:10.3748/wjg.v25.i44.6527
15. Fink SL, Cookson BT. Caspase-1-dependent pore formation during pyroptosis leads to osmotic lysis of infected host macrophages. *Cell Microbiol*. 2006;8(11):1812–1825. doi:10.1111/j.1462-5822.2006.00751.x
16. Deng J, Tan W, Luo Q, Lin L, Zheng L, Yang J. Long non-coding RNA *MEG3* promotes renal tubular epithelial cell pyroptosis by regulating the miR-18a-3p/GSDMD pathway in lipopolysaccharide-induced acute kidney injury. *Front Physiol*. 2021;12:663216. doi:10.3389/fphys.2021.663216
17. Xue R, Yang J, Jia L, et al. Mitofusin2, as a protective target in the liver, controls the balance of apoptosis and autophagy in acute-on-chronic liver failure. *Front Pharmacol*. 2019;10:601. doi:10.3389/fphar.2019.00601
18. Thakur V, Sadanandan J, Chattopadhyay M. High-mobility group box 1 protein signaling in painful diabetic neuropathy. *Int J Mol Sci*. 2020;21(3):881. doi:10.3390/ijms21030881
19. Paudel YN, Angelopoulou E, Semple B, Piperi C, Othman I, Shaikh MF. Potential neuroprotective effect of the HMGB1 inhibitor glycyrrhizin in neurological disorders. *ACS Chem Neurosci*. 2020;11(4):485–500. doi:10.1021/acschemneuro.9b00640
20. Wannamaker W, Davies R, Namchuk M, et al. (S)-1-((S)-2-{[1-(4-amino-3-chloro-phenyl)-methanoyl]-amino}-3,3-dimethyl-butanoyl)-pyrrolidine-2-carboxylic acid ((2R,3S)-2-ethoxy-5-oxo-tetrahydro-furan-3-yl)-amide (VX-765), an orally available selective interleukin (IL)-converting enzyme/caspase-1 inhibitor, exhibits potent anti-inflammatory activities by inhibiting the release of IL-1beta and IL-18. *J Pharmacol Exp Ther*. 2007;321(2):509–516. doi:10.1124/jpet.106.111344
21. Li F, Xu M, Wang M, et al. Roles of mitochondrial ROS and NLRP3 inflammasome in multiple ozone-induced lung inflammation and emphysema. *Respir Res*. 2018;19(1):230. doi:10.1186/s12931-018-0931-8
22. Huang J, Huang X, Chen Z, Zheng Q, Sun R. Dose conversion among different animals and healthy volunteers in pharmacological study. *Chin J Clin Pharmacol Ther*. 2004;09:1069–1072.
23. Schindelin J, Arganda-Carreras I, Frise E, et al. Fiji: an open-source platform for biological-image analysis. *Nat Methods*. 2012;9(7):676–682. doi:10.1038/nmeth.2019
24. Triantafyllou E, Woollard KJ, McPhail MJW, Antoniades CG, Possamai LA. The role of monocytes and macrophages in acute and acute-on-chronic liver failure. *Front Immunol*. 2018;9:2948. doi:10.3389/fimmu.2018.02948
25. Yuan S, Liu Z, Xu Z, Liu J, Zhang J. High mobility group box 1 (HMGB1): a pivotal regulator of hematopoietic malignancies. *J Hematol Oncol*. 2020;13(1):91. doi:10.1186/s13045-020-00920-3
26. Kolios G, Valatas V, Kouroumalis E. Role of kupffer cells in the pathogenesis of liver disease. *World J Gastroenterol*. 2006;12(46):7413–7420. doi:10.3748/wjg.v12.i46.7413
27. Cao Z, Li F, Xiang X, et al. Circulating cell death biomarker: good candidates of prognostic indicator for patients with hepatitis B virus related acute-on-chronic liver failure. *Sci Rep*. 2015;5(1):14240. doi:10.1038/srep14240
28. Zhou R, Zhao S, Zou M, et al. HMGB1 cytoplasmic translocation in patients with acute liver failure. *BMC Gastroenterol*. 2011;11(1):21. doi:10.1186/1471-230X-11-21
29. Liu X, Lu B, Fu J, Zhu X, Song E, Song Y. Amorphous silica nanoparticles induce inflammation via activation of NLRP3 inflammasome and HMGB1/TLR4/MYD88/NF-kb signaling pathway in HUVEC cells. *J Hazard Mater*. 2021;404(PtB):124050. doi:10.1016/j.jhazmat.2020.124050
30. Xu Q, Zhao B, Ye Y, et al. Relevant mediators involved in and therapies targeting the inflammatory response induced by activation of the NLRP3 inflammasome in ischemic stroke. *J Neuroinflammation*. 2021;18(1):123. doi:10.1186/s12974-021-02137-8
31. Kelley N, Jeltema D, Duan Y, He Y. The NLRP3 Inflammasome: an overview of mechanisms of activation and regulation. *Int J Mol Sci*. 2019;20(13):3328. doi:10.3390/ijms20133328
32. Ghoneim ME, Abdallah DM, Shebl AM, El-Abhar HS. The interrupted cross-talk of inflammatory and oxidative stress trajectories signifies the effect of artesunate against hepatic ischemia/reperfusion-induced inflammasomopathy. *Toxicol Appl Pharmacol*. 2020;409:115309. doi:10.1016/j.taap.2020.115309
33. Wang M, Chen X, Zhang Y. Biological functions of gasdermins in cancer: from molecular mechanisms to therapeutic potential. *Front Cell Dev Biol*. 2021;9:638710. doi:10.3389/fcell.2021.638710
34. Wang K, Sun Q, Zhong X, et al. Structural mechanism for GSDMD targeting by autoprocessed caspases in pyroptosis. *Cell*. 2020;180(5):941–955. doi:10.1016/j.cell.2020.02.002
35. Wang W, Zhang T. Caspase-1-mediated pyroptosis of the predominance for driving CD4+ T cells death: a nonlocal spatial mathematical model. *Bull Math Biol*. 2018;80(3):540–582. doi:10.1007/s11538-017-0389-8
36. Chevriaux A, Pilot T, Derangère V, et al. Cathepsin B is required for NLRP3 inflammasome activation in macrophages, through NLRP3 interaction. *Front Cell Dev Biol*. 2020;8:167. doi:10.3389/fcell.2020.00167
37. Wang J, Wang L, Zhang X, et al. Cathepsin B aggravates acute pancreatitis by activating the NLRP3 inflammasome and promoting the caspase-1-induced pyroptosis. *Int Immunopharmacol*. 2021;94:107496. doi:10.1016/j.intimp.2021.107496
38. Xia P, Pan Y, Zhang F, et al. Pioglitazone confers neuroprotection against ischemia-induced pyroptosis due to its inhibitory effects on HMGB-1/RAGE and Rac1/ROS pathway by activating PPAR-ɤ. *Cell Physiol Biochem*. 2018;45(6):2351–2368. doi:10.1159/000488183
39. Yu P, Zhang X, Liu N, Tang L, Peng C, Chen X. Pyroptosis: mechanisms and diseases. *Signal Transduct Target Ther*. 2021;6(1):128. doi:10.1038/s41392-021-00507-5
40. Wang L, Qin X, Liang J, Ge P. Induction of pyroptosis: a promising strategy for cancer treatment. *Front Oncol*. 2021;11:635774. doi:10.3389/fonc.2021.635774